

Dynamical Global Downscaling of Global Reanalysis

Kei Yoshimura^{1,2} and Masao Kanamitsu¹

¹Scripps Institution of Oceanography, University of California, San Diego

²Institute of Industrial Science, The University of Tokyo

Submitted to Monthly Weather Review

As of 2007/06/08

Corresponding author:

Kei Yoshimura (klyoshimura@ucsd.edu),

CRD/SIO/UCSD MC0224, 9500 Gilman Dr., La Jolla, CA92093-0224, USA

ABSTRACT

Aiming at producing higher resolution global reanalysis datasets from coarse 200 km resolution reanalysis, a global version of the dynamical downscaling using a global spectral model (GSM) is developed. A variant of spectral nudging, the scale-selective bias correction (SSBC) developed for regional models is modified in the following manner to adapt it to the global domain; 1) temperature is nudged in addition to the zonal and meridional components of winds, 2) a new formulation of the nudging coefficient is proposed in place of a single constant coefficient, 3) perturbation of zonally averaged humidity is set to zero, instead of area average. The downscaling was performed using T248L28 (about 50 km resolution) global model for 2001, driven by NCEP/NCAR Reanalysis 2 (T62L28 resolution). Evaluation with high-resolution observations showed that the monthly averaged surface temperature and daily variation of precipitation become better than the Reanalysis over the globe, although a significant positive bias of global precipitation was observed in the downscaled simulation. Over North America, surface wind speed and temperature become better, and over Japan, the diurnal pattern of surface temperature is much improved, as are wind speed and precipitation, but not humidity. Three well-known synoptic/sub-synoptic scale weather patterns over the USA, Europe, and Antarctica were shown to become more realistic with reasonable temperature- wind-topography relations. This study suggests that the global downscaling is a viable and economical method to obtain high-resolution reanalysis without re-running a very expensive high-resolution full data assimilation.

1. Introduction

Reanalysis is now an indispensable dataset for climate studies. It provides analysis of a variety of variables, which are internally consistent within the framework of the numerical model used in the data assimilation. However, its coarse spatial resolution has been problematic for various application studies, such as the regional impact of climate change on agriculture (Fuhrer et al., 2006), river flows (Wilby et al., 1999 and Miller et al., 2003), terrestrial water and energy cycle (Dirmeyer et al., 2006), water resources estimation with anthropogenic impacts (Oki and Kanae, 2006, Lehner et al., 2006), and many others.

The coarseness of the reanalysis resolution is mainly due to the computational burden. For example, one analysis by a typical data assimilation requires computer time approximately equivalent to a 4-5 day forecast. Since reanalysis involves analyzing a very long period of data (40 plus years) in a reasonable time (normally within 3-5 years), limiting the analysis resolution is unavoidable.

One approach to this problem is the use of regional data assimilation. NCEP (National Centers for Environmental Prediction) recently performed regional reanalysis over the United States for the period 1979 to present using 32 km resolution (Mesinger et al., 2006). European countries are also working together on a similar project (EURRA, 2005). While this approach is feasible, such efforts are limited to a small number of countries and institutions with advanced data assimilation systems and large computer power.

Dynamical downscaling is an alternative to regional data assimilation. As already pointed out by von Storch et al. (2000), dynamical downscaling with the

spectral nudging technique is considered a “poor person’s data assimilation technique.” Some comparisons between regional data assimilation and dynamical downscaling have been studied by Kanamaru and Kanamitsu (2007a). It was concluded that the dynamical downscaling with higher spatial resolution has an advantage over the coarser resolution data assimilation. Part of the reason for this is the current data assimilation system’s inability to effectively utilize high-density near-surface observations, which places more weight on the initial guess produced by the high-resolution numerical model.

In spite of its economical merit, a regional climate model is inherently mathematically ill-posed due to specified lateral boundary values, which result in noises and instabilities that propagate into the interior of the domain and contaminate the downscaled analysis. In addition, we lose large areas around the lateral boundaries due to lateral boundary nudging.

Furthermore, in the recently proposed transferability intercomparisons, Rockel et al. (2006) proposed a comparison of regional simulations with fixed model parameterizations over several globally-distributed domains to test the model performance and to improve model parameterizations. The project targets regional models, but if similar experiments can be performed using a global model, this could be ideal for regional comparison since the simulation would not be contaminated by lateral boundaries. Global downscaling is much more economical than running the regional model at multiple locations.

In this study, a global version of the dynamical downscaling using a global spectral model and spectral nudging, aiming at producing finer resolution global datasets from 200 km resolution reanalysis, is developed. For this purpose, a

modified version of the scale-selective bias correction (Kanamaru and Kanamitsu, 2007a), is employed. The major objective of this paper is to demonstrate that a “global high-resolution” version of the NCEP global Reanalysis can be produced with relatively low computer cost.

A different type of global downscaling was recently conducted by Ghan et al. (2006). They downscaled a GCM (general circulation model) simulation with a physically based subgrid orography scheme over global terrain for a multi-decadal period. In their method, surface variables in each coarse grid cell are redistributed into finer subgrids considering elevation effect, but with rather crude airflow dynamics within a grid, and an offline-mode of a land surface model is driven by these surface variables. Therefore, their method is not fully dynamical downscaling, but rather a practical and computationally inexpensive approach to global downscaling.

This paper is outlined as follows. Section 2 describes a global version of the spectral nudging technique, specifically, the modification of the scale-selective bias correction method, and the results of the preliminary short-term nudging experiments are shown. Section 3 presents results from a finer longer-term downscaling experiment. The results are evaluated against observations over the globe and over specific regions. Finally, the last section provides a summary and conclusions.

2. Method

a. Modification of SSBC for a global spectral model

The scale-selective bias correction (SSBC) scheme for a regional spectral model (RSM) developed by Kanamaru and Kanamitsu (2007a; KK07 hereafter) is

used as a base for this study, but it is modified for the global spectral model (GSM). The GSM used for this study is based on the medium range forecast (MRF) model used at NCEP for making operational analysis and predictions (see Caplan et al, 1997). The GSM used in this study and the RSM used in developing KK07 were both originally developed at NCEP, and have almost identical physical and dynamical processes (Juang et al., 1997). The SSBC must be modified due to differences in the spectral base functions used in GSM and RSM. The global coverage that includes tropics and extra-tropics also calls for the modification of the SSBC.

Prior to the downscaling process, driving reanalysis data are pre-processed; surface pressure is recalculated for higher resolution topography in the high-resolution global model with the hydrostatic relationship, and temperature, humidity, and wind fields are vertically interpolated/extrapolated to the new model sigma levels. This process is basically the same as that of the RSM-SSBC's correction for surface pressure.

In the RSM, the sine and cosine series for both x - and y -directions are used as base functions, and nudging is applied directly to the two dimensional sine and cosine amplitudes. In GSM, the base function is a spherical harmonics, and the SSBC equivalent of RSM is to apply the damping to the amplitude of total wavenumber. However, this implies that the scale of the fields to be damped is uniform in the zonal and meridional directions, but in reality, it is desirable to damp the scale differently for zonal and meridional directions based on the atmospheric characteristics of the long waves, which tend to have larger scale in east-west than in north-south. For this reason, SSBC for a specified zonal scale is applied at each

Gaussian latitude. The equations for damping are described as follows:

$$f_{(\lambda,\phi)} = \sum_{m=-M}^{m=M} F_{(m,\phi)} e^{im\lambda}$$

$$F_{(m,\phi)} = \begin{cases} F_{f(m,\phi)} & (|m| > \frac{2\pi R_E \cos \phi}{L}) \\ \frac{1}{\alpha + 1} (F_{f(m,\phi)} + \alpha F_{a(m,\phi)}) & (|m| \leq \frac{2\pi R_E \cos \phi}{L}) \end{cases} \quad (1)$$

where f is a physical variable, F is the Fourier coefficient, and the subscript f and a indicate forecast and analysis (driving data), respectively. λ , ϕ , R_E , m and M indicate longitude, latitude, radius of the earth, wavenumber, and the truncation wave number, respectively. α is a nudging coefficient, and L is a nudging scale where waves longer than L will be nudged.

The original SSBC applied to RSM uses zonal and meridional wind components at all sigma levels to be nudged towards coarse resolution reanalysis field by using a single weighting coefficient ($\alpha=0.9$). KK07 named this correction UV damping and applied it only to waves whose physical wavelengths are 1000 km or longer ($L=1000$ km). In GSM-SSBC however, preliminary experiments are first conducted to find the sensitivities of the simulation to the nudging parameter and to other related parameters, the results being described in the next section and in the appendix.

In addition, the area average correction in the RSM, which sets the difference between regional area averages of temperature and humidity between reanalysis and downscaling to zero (TQ correction), is modified to set zonal averaged temperature and humidity to zero to preserve the meridional gradient of the zonal mean in the reanalysis.

b. Preliminary Experiments for Retaining Large-scale Feature

1) DESIGN OF THE EXPERIMENTS

Results from several preliminary experiments with the new GSM-SSBC, which are listed in Table 1, are presented. An experiment with a similar setting to the RSM-SSBC (“UV damping” with $\alpha=0.9$ and $L=2000$ km) is the control experiment (CTL). A larger critical scale “ L ” than the one used in RSM (1000 km) is chosen based on the fact that the global downscaling covers large ocean areas where observation is sparse and thus the accuracy of the reanalysis diminishes. $L=1000$ is also tested to see the sensitivity of the results, which is shown in the appendix. The experiment with “UV and T damping” with $\alpha=0.9$ and $L=2000$ km is named TEMP1. Note that the TEMP1 experiment serves to test the need for nudging temperature, which was not applied in the regional downscaling. Besides TEMP1, an additional experiment, TEMP2, that utilizes nudging coefficient $\beta_{(m,\phi)}$ which varies with latitude, is performed:

$$\beta_{(m,\phi)} = \sqrt{1 - \frac{mL}{2\pi R_E \cos \phi}}$$

$$F_{(m,\phi)} = \begin{cases} F_{f(m,\phi)} & (|m| > \frac{2\pi R_E \cos \phi}{L}) \\ (1 - \beta_{(m,\phi)})F_{f(m,\phi)} + \beta_{(m,\phi)}F_{a(m,\phi)} & (|m| \leq \frac{2\pi R_E \cos \phi}{L}) \end{cases} \quad (2)$$

where m is zonal wavenumber, R_E is the radius of the earth and ϕ is latitude. It gives smoother nudging weight from large to short wavelengths and eventually no weight at the nudging scale L . Note that it is equivalent to changing α from a large value ($\alpha=40$ on the equator with the largest wavelength, $m=1$) to 0 at L . Additionally, experiments with different constant α , namely ALP05 and ALP2, are also shown in the appendix. All these experiments are performed using the same model configurations: the T126 (about 100 km) and 28 sigma levels as a downscaling model;

6-hourly snapshots of prognostic variables from NCEP Reanalysis 2 (R2; Kanamitsu et al., 2002) with a resolution of T62 and 28 levels as a lateral forcing; and 10 day integration starting at the beginning of March 1990 using interpolated Reanalysis as initial conditions. It should be noted that the GSM land surface process and convective scheme are different from those of R2. This study used the Noah land surface model and Relaxed Arakawa-Schubert convection scheme (Moorthi and Suarez, 1992) whereas R2 used the OSU land surface model and Simplified Arakawa-Schubert convection scheme (Pan and Wu, 1994)).

2) RESULTS OF THE EXPERIMENTS

In Figure 1, the power spectra of global kinetic energy at two different sigma levels are shown with those of R2 (up to total wavenumber $n=62$), CTL, TEMP1, TEMP2, and forecast (FCST) (up to $n=126$). FCST is a run without any nudging applied. The computation of the spherical harmonic spectra by Koshyk and Hamilton (2001) is followed. For the wavenumber less than 20, the power spectra of R2 and CTL are almost identical, indicating that the large-scale nudging is working correctly at both levels (wavenumber 20 corresponds to about 2000 km wavelength at the equator). It is interesting to note that the FCST spectra deviate from those of R2 at small wavenumbers after 10 days indicating deviation from analysis in the large scale if no nudging is applied.

For the wavenumbers larger than 20, the difference between R2 and CTL becomes apparent. Particularly for R2, the spectra quickly drop down around wavenumber 40, but CTL keeps its monotonical decrease up to wavenumber 120 at low levels and 90 at upper levels. This energy gain between 40 and 120 indicates that the dynamical downscaling is producing realistic small scales. In addition, the

spectra of CTL and FCST for wavenumbers larger than 20 stay almost the same. This implies that the large-scale nudging is working and is not significantly impacting the small scale generated by the high-resolution model.

Although the energy spectra seem to be reasonable in CTL, large scale systematic deviation from Reanalysis in the height field in the stratosphere was found (Figure 2). The systematic error is made of wavenumbers 1 and 2 with its maximum at the equator. From further investigations, it is found that this large scale systematic error is created by the global model used in the downscaling. It is also found that, even in the R2 assimilation, a very similar systematic error is created in the 6 hour forecast guess, which is corrected by the objective analysis. Leaving the temperature field unnudged enhances the bias, amplifying it to 3 - 4 degrees Kelvin in several days. The corresponding error in height reaches 60-80 m. The cause of this problem is unclear and finding it is beyond the scope of this paper. Such a significant bias in height has not been found in previous dynamical downscaling studies using RSMs (Kanamaru and Kanamitsu, 2007a, 2007b). This is partly because the horizontal scale of the systematic error is simply larger than the regional domain, and a correction of area averaged temperature is enough to fix the problem. Another reason might be that the downscaling is performed in extra-tropical latitudes where UV damping is sufficient to control temperature bias.

TEMP1 and TEMP2 experiments are performed in order to suppress the large-scale temperature error in the tropics. The results are illustrated in Figure 3, which shows vertical profiles of global root mean square difference (RMSD) of geopotential height between the experiments and the forcing (R2). As expected, large-scale systematic bias in the stratosphere is diminished in both TEMP1 and

TEMP2, and the global RMSDs are dramatically decreased compared to CTL. It should be noted that the RMSD also decreases in the entire troposphere. The departures of geopotential height from the reanalysis in TEMP1 are about 10 m at all pressure levels which is still large relative to KK07 (about 2-5 m), whereas in TEMP2 they are satisfactorily within about 4 to 6 m.

The kinetic energy spectra are quite similar to those of CTL (see Figure 1), as is humidity (figure not shown), indicating that the nudging of temperature did not cause any dynamical distortion. Thus the TEMP2 setting is chosen as the default for GSM-SSBC.

3. A 50 km Global Downscaling

In the previous section, it was confirmed that the large-scale dynamical features in the reanalysis were successfully retained in the global downscaling. In this section, it is examined how downscaled fields improve the fit to observations in a longer downscaling run. For this purpose, a global downscaling by T248 (about 50 km) resolution model was conducted (experiment named T248) for the year 2001. The nudging scheme used in TEMP2 was adopted. The settings of the experiment are the same as those in the previous section; the number of sigma levels is set to 28 and T62L28 6-hourly NCEP R2 is used for forcings. Considering the spin-up of land surface parameters, the model is run from 1998, but the results of 2001 are shown below.

a. Global Evaluation

1) GLOBAL TEMPERATURE COMPARED WITH CRU

Figure 4 shows globally downscaled monthly mean temperature over land compared with the CRU (Climate Research Unit) dataset (version TS 2.1, Mitchell

and Jones, 2005). From Figure 4d and 4e, it is found that the Arctic Islands, the extreme northern part of North America, and the eastern part of Siberia are slightly warmer in both R2 and the downscaled analysis. There are slightly cooler biases in Central Africa, the Sahel, and the Amazon Basin. However, there is an obvious improvement associated with global downscaling due to more realistic surface topography especially over mountain ranges. The clearest difference is seen in the Tibetan Plateau and in the Andes, but there are also improvements over the Pacific Coastal Ranges, the Alps, the Ethiopian Plateau, the Mongolian Plateau, and many other locations.

2) GLOBAL PRECIPITATION COMPARED WITH GPCP AND CRU

In Figure 5, the downscaled analysis and original reanalysis R2 (T62 resolution) monthly precipitation are compared with those of GPCP (Huffman et al., 2001), CRU, and FCST during January and July 2001. Seasonal evolutions over the major continents are clearly simulated well, but they are already well simulated in R2. In both months spatial contrasts associated with topography and coastlines become more apparent in the downscaled analysis, for example, in the Himalaya and Sierra Madre Ranges, the Coast Ranges in British Columbia, and the western coastline of India.

More interesting features can be seen over oceans. Roughly speaking, the distribution in the Northern Hemisphere in the simulations agrees with that of GPCP, such as the narrow ITCZ over the Pacific and Atlantic and their seasonal shift, the wide coverage of large precipitation over the northern Pacific in January and its westward recession in July with less precipitation over the eastern half of the region and Asian Monsoon seasonality. In the Southern Hemisphere however, the

downscaled analysis shows erroneous double-ITCZ in the southern Pacific and the southern Atlantic whereas no such errors are found in FCST. These ITCZs were also seen in R2, but they became more distinct in the downscaling run. From the difference between R2, T248, and FCST, it can be concluded that significant and large-scale errors already existed in the R2 analysis fields, and they somehow become amplified in the global downscaling.

Figure 6 shows the seasonal variation of monthly global mean precipitation compared with GPCP, CRU, and R2. It shows a significant precipitation increase over the whole globe throughout the year. The increase in precipitation due to the increase in model resolution has been noted by Duffy et al. (2003) for global model and by Murphy (1999), Misra et al. (2002) and Meinke et al. (2007) for regional model. Reduction of excessive precipitation can be achieved by tuning parameterizations (Mizota et al., 2006) or by improving physical processes, but was not performed in this study in order to make the comparison with Reanalysis more straightforward.

Figure 7 shows the global distribution of correlation coefficients of daily precipitation against 1 degree GPCP during January and July, 2001. As a common feature, there are zonal bands of high correlation over mid and high latitude in both hemispheres, and low correlation over the tropical regions. Differences of the correlation for R2 and the downscaled analysis are not so clear from the figure, but the global average of the correlations is better for downscaled analysis throughout the year, as shown in Figure 8.

b. Regional Evaluation in detail

One of the advantages of global downscaling is that we can examine any

regional areas over the globe for evaluation. In this section, two regions, North America and Japan, where regional scale observation is readily available, are investigated.

1) VALIDATION OVER NORTH AMERICA WITH NORTH AMERICAN REGIONAL REANALYSIS (NARR)

In Figure 9, monthly mean wind speed for July 2001 is compared with NARR (Mesinger et al., 2006). NARR is a data assimilation product using the 32 km resolution Eta model. The larger wind speed in most of the Pacific side of the continent is reduced to the level of NARR in the downscaled results, particularly for Alaska and British Columbia, the west coast of the U.S., and Baja California. A similar reduction is also seen in northern Texas and Oklahoma.

Figure 10 shows deviation of daily mean 2-meter temperature from the monthly averages on July 29, 2001. Large-scale anomalies, such as the cold anomaly in western Canada, the Labrador Peninsula, and the west and east coasts of the U.S. and the warm anomaly in Alaska, Greenland, the central U.S. and Canada, is common in these three panels, but in R2 (Fig. 10a), cold regions appear more distinctively than those of NARR (Fig. 10c), such as in northern Mexico and the southern U.S.. In the T248 downscaling (Fig. 10b), the distribution becomes more similar to that of NARR, closer to observation. The reason for the improvement is probably due to the fact that the regions are characterized by complex geography, such as the Gulf of California, the Sierra Madres in northern Mexico and the Great Plains in the U.S., where the dominant scale tends to be much smaller than the forced scale of 2000 km.

2) VALIDATION OVER JAPAN WITH AMEDAS

Now our results are compared with more than 1000 Automated Meteorological Data Acquisition System (AMeDAS) in-situ meso-scale surface observatories covering all of Japan, for wind speed, humidity, temperature, and precipitation. The average AMeDAS station location interval is about 20 km, and most observations are hourly. The AMeDAS data are first interpolated to 0.1 degree (10 km) latitude-longitude coordinate grids with topographic correction using standard lapse rate and then compared it with the downscaled analysis.

Figure 11 shows the distribution of correlation coefficient of the four surface variables between the downscaled analysis and AMeDAS in January and July 2001. There is clearly a large improvement in January precipitation (see Fig.11a, 11n), and a somewhat smaller improvement in temperature fields for both months (see Fig.11e-h). By averaging the coefficients over the region for all months, it is found that the wind speed, temperature, and precipitation of the downscaled analysis became closer to the AMeDAS observations than those of Reanalysis. Only the humidity fields stayed similar to R2.

In Figure 12, a single grid point at 140.0E and 36.0N (near Tsukuba, Japan) is chosen and the temporal variation of the variables (a) wind speed, (b) temperature, (c) humidity, and (d) precipitation for the first 10 days in July 2001 are shown. We can see from this figure that the improvement of correlation coefficient in Figure 11 was from better reproduction of diurnal variations for wind speed and temperature. The diurnal cycle of absolute humidity is weak, but other fluctuations were better reproduced in the T248 downscaling. In precipitation, the downscaled analysis captured a rain event on 6 July, 2001, which was very sharp and short according to the observation, whereas R2 did not have any precipitation in that period.

3) SYNOPTIC/SUB-SYNOPTIC SCALE WEATHER PATTERNS

In this section, several typical intense synoptic- and subsynoptic-scale atmospheric phenomena are selected and the downscaled analysis is compared with the corresponding coarse resolution Reanalysis. A Santa Ana wind event in Southern California, a Mistral in West Europe, and the katabatic wind in Antarctica are shown. Figure 13 shows daily snapshots of temperature anomaly (deviation from monthly mean), wind, and surface elevation of those events for R2 and the downscaled analysis.

The Santa Ana is a warm, dry northeasterly wind in Southern California during fall and winter. Typical features of the Santa Ana can be found in many works (e.g., Hu and Liu, 2003). An example of a Santa Ana event on January 3, 2001 is shown here. Both R2 (Fig.13a) and the downscaled analysis (Fig.13b) capture high temperatures along the coast of Southern California, but the downscaled analysis shows more detailed wind patterns associated with the complex topography of Sierra Nevada, whereas winds in R2 are more uniform without many topographical features.

The Mistral is a cold, strong northwesterly in southern France and Sardinia which occurs during winter to spring. Figure 13c, d shows R2 and the downscaled winds and temperature on 22 December 2001. General characteristics of the phenomenon, such as the cold northwesterly in the southern coast of France, are captured in R2, but more detailed features are found in the downscaled analysis, *i.e.*, colder and stronger northwesterlies which are more regionalized over the area from the western edge of the Alps to north of the Pyrénées. It should be noted that warm temperature anomalies in R2 in the middle of France, Germany and Switzerland

disappeared in the downscaled analysis, due to the enhancement of cold anomalies in the southern part of France.

A katabatic wind is a prominent feature of the surface wind system over Antarctica. Figure 13e shows temperature and wind in R2 over the Antarctic Peninsula, and coastal katabatic winds are not apparent. In the downscaled analysis, however, prominent katabatic winds appear over the eastern coast of the peninsula. This difference looks quite remarkable. However, it should be mentioned that large-scale katabatic winds are already reasonably well simulated in the coarse resolution reanalyses over flat terrain and slopes, such as over the coastline of Eastern Antarctica (Parish and Cassano, 2001), and the improvement in the downscaled analysis is not so significant over those areas. Since the width of the Antarctic Peninsula is at most 500 km with complex topography, the downscaling was capable of producing small-scale details that R2 could not represent.

4. Summary and Conclusions

In this study, an attempt has been made to develop a global version of the dynamical downscaling using the global spectral model (GSM) with a spectral nudging technique. A modified version of the scale-selective bias correction (SSBC) (Kanamaru and Kanamitsu, 2007a) is applied. The global downscaling is free of the lateral boundary noise from which regional global models suffer, and can be considered a way to produce computationally efficient high-resolution global reanalysis datasets from coarse resolution data assimilation analysis.

SSBC was modified for GSM in three different ways. First, the large-scale temperature of the scale greater than 2000 km was nudged in addition to the zonal and meridional components of wind. This was necessary to reduce the large-scale

temperature bias in the stratosphere in equatorial tropics. Second, a new functional form of the nudging coefficient was proposed to replace the single constant coefficient used in SSBC. This coefficient gives smoother nudging from large to short wavelengths. Third, the zonally averaged humidity was replaced with those of the reanalysis. With this nudging scheme, large-scale features of the reanalysis are well maintained in the downscaling. The departures of geopotential height of downscaled analysis from reanalysis are in a range of 4 to 6 meters at all of the pressure levels.

GSM-SSBC was applied to a T248L28 (about 50 km resolution) global model and global downscaling was performed for the entire year of 2001, using T62L28 NCEP/NCAR R2 as a large-scale forcing. Surface variables and precipitation were compared with R2 and available high-resolution observations, *i.e.*, CRU, GPCP, NARR, and AMeDAS. The global temperature fields compared with CRU temperature showed that the downscaled analysis better matched with observation due to the better topography. Monthly averaged precipitation, its seasonality and daily variation were compared with those of CRU and GPCP. The downscaled precipitation had a positive bias in many of the high-resolution simulations, but the daily variability was better reproduced in the downscaled analysis than in the R2 throughout the year.

Comparisons with NARR over North America showed that the downscaled surface wind speed and temperature are closer to NARR than the Reanalysis to NARR. Over Japan, the comparison with more than 1000 AMeDAS in-situ observations showed that the downscaled analysis fits better to observation than R2 for surface temperature, wind speed, and precipitation. The fit of humidity was not

significantly improved. The improvement of diurnal variation of surface temperature was significant.

In addition, three typical synoptic/sub-synoptic scale weather features were selected for comparison, namely the Santa Ana in Southern California, the Mistral in Southern France, and katabatic winds in Antarctica. They clearly showed realistic regional-scale features with respect to temperature and wind.

One of the purposes of this study is to determine whether this global downscaling can serve as a replacement of the global high-resolution reanalysis without performing an expensive high-resolution global data assimilation. From the present result, this seems to be the case at least for surface meteorological variables and precipitation. However, in order to confirm this, it is also necessary to investigate the fit of the downscaling to observations in the free atmosphere and to compare the results with the high-resolution data assimilation analysis. Since this would require a full objective analysis system capable of using high-density surface observation, it is beyond our capability at this time. Some of the deficiencies of the downscaled analysis, such as the positive bias in precipitation and the double ITCZ can be improved by introducing better convective parameterization and cloud water prediction schemes. Since this paper is a feasibility study of the global downscaling, those improvements are left to future work.

Acknowledgments:

A part of this research is funded by the Japan Society for the Promotion of Science Postdoctoral Fellowships for Research Abroad. This study was also partially supported by NSC 95-211-M133 -001 -AP4 and NOAA NA17RJ1231. The views

expressed herein are those of the authors and do not necessarily reflect the views of NOAA. We would like to thank Drs. H. Kanamaru and J. Roads for their constructive comments and assistance, Ms. C. Papadopoulos for her technical help with computational resources, and Ms. D. Boomer for her assistance in proof-reading.

APPENDIX

Sensitivity Experiments of L and α

Some additional experiments are performed using the same environmental setting as those described in section 2 for evaluating sensitivities of the nudging scale L and the weighting coefficient α . Experiments similar to CTL and TEMP2 but with $L=1000$ km are named L1000 and L1000F, respectively. Experiments similar to TEMP1 with different α , namely $\alpha=0.5$ and 2.0, are named as ALP05, and ALP2, respectively. As shown in Figure A, the sensitivities of downscaling to both L and α are not significant. The comparison between CTL and L1000 and between TEMP2 and L1000F indicates that the result of the 2000 km nudging scale is sufficiently similar to that of 1000 km. The 2000 km scale was chosen as our default considering the accuracy of Reanalysis data over ocean and tropics as noted in the main text. As to the form of the nudging coefficients, ALP2 is almost identical to TEMP1 and ALP05 is worse than TEMP1, implying that it is difficult to significantly decrease the RMSD by adjusting the constant nudging coefficient. Therefore, the TEMP2 setting was adopted in our experiment.

REFERENCES

- Caplan, P., J. Derber, W. Gemmil, S.-Y. Hong, H.-L. Pan and D. Parrish, 1997: Changes to the 1995 NCEP operation medium-range-forecast model analysis-forecast system, *Weather Forecast*, **12**, 581-594.
- Dirmeyer, P.A., X. Gao, M. Zhao, T. Oki, N. Hanasaki, 2006: The second global soil wetness project (GSWP-2), *Bull. Amer. Meteor. Soc.*, **87**, 1381-1397.
- Duffy, P.B., B. Govindasamy, J.P. Iorio, J. Milovich, K.R. Sperber, K.E. Taylor, M.F. Wehner, S.L. Thompson, 2003: High-resolution simulations of global climate, part 1: present climate, *Climate Dyn.*, **21**, 371-390.
- European Regional Reanalysis project (EURRA), 2005: Meeting Report on Workshop to discuss a potential European Regional Reanalysis project (EURRA).
- Fuhrer, J., M. Beniston, A. Fischlin, Ch. Frei, S. Goyetter, K. Jasper, Ch. Pfister, 2006: Climate risks and their impact on agriculture and forests in Switzerland, *Climatic Change*, **79**, 79-102.
- Ghan, S.J., T. Shippert, and J. Fox, 2006: Physically based global downscaling: regional evaluation, *J. Climate*, **19**, 429-445.
- Hu, H. and T. Liu, 2003: Oceanic thermal and biological responses to Santa Ana winds, *Geophys. Res. Lett.*, **30**, 1596, doi:10.1029/2003GL017208.
- Huffman, G.J., R.F. Adler, M.M. Morrissey, D.T. Bolvin, S. Curtis, R. Joyce, B. McGavock, and J. Susskind, 2001: Global precipitation at one-degree daily resolution from multisatellite observation, *J. Hydromet.*, **2**, 36-50.
- Juang, H.-M.H, S.-Y. Hong, and M. Kanamitsu, 1997: The NCEP regional spectral model: an update, *Bull. Amer. Meteor. Soc.*, **78**, 2125-2143.
- Kanamaru, H. and M. Kanamitsu, 2007a: Scale-selective bias correction in a

- downscaling of global analysis using a regional model, *Mon. Wea. Rev.*, **135**, 334-350.
- Kanamaru, H., and M. Kanamitsu, 2007b: Dynamical downscaling of global analysis/simulation over the Northern Hemisphere, submitted to *Mon. Wea. Rev.*
- Kanamitsu, M., W. Ebisuzaki, J. Woolen, J. Potter, and M. Fiorino, 2002: NCEP/DOE AMIP-II Reanalysis (R-2), *Bull. Amer. Meteor. Soc.*, **83**, 1631-1643.
- Koshyk, J.N. and K. Hamilton, 2001: The horizontal kinetic energy spectrum and spectral budget simulated by a high-resolution troposphere-stratosphere-mesosphere GCM, *J. Atmos. Sci.*, **58**, 4, 329-348.
- Lehner B., P. Döll, J. Alcamo, T. Henrichs, F. Kaspar, 2006: Estimating the Impact of Global Change on Flood and Drought Risks in Europe: A Continental, Integrated Analysis, *Climatic Change*, **75**, 273-299.
- Meinke, I., J. Roads, and M. Kanamitsu, 2007: Global evaluation of the RSM simulated precipitation through transferability studies during CEOP, *J. Meteor. Soc. Japan*, in print.
- Mesinger, F., and co-authors, 2006: North American regional reanalysis, *Bull. Amer. Meteor. Soc.*, **87**, 343-360.
- Misra, V., P.A. Dirmeyer, B.P. Kirtman, H.-M. Henry Juang, M. Kanamitsu, 2002: Regional simulation of interannual variability over South America, *J. Geophys. Res.*, **107**, D20, DOI 10.1029/2001JD900216.
- Miller, N.L., K.E. Bashford, and E. Strem, 2003: Potential impacts of climate change on California hydrology, *J. Amer. Water Resour. Assoc.*, **39**, 771-784.
- Mitchell, T.D. and P.D. Jones, 2005: An improved method of constructing a database

- of monthly climate observations and associated high-resolution grids, *Int. J. Climatol.*, **25**, 693-712.
- Mizota, R., K. Oouchi, H. Yoshimura, A. Noda, K. Katayama, S. Yukimoto, M. Hosaka, S. Kusunoki, H. Kawai, and M. Nakagawa, 2006: 20-km-mesh global climate simulations using JMA-GSM model —mean climate states—, *J. Meteor. Soc. Japan*, **84**, 165-185.
- Moorthi, S., and M.J. Suarez, 1992: Relaxed Arakawa-Schubert: a parameterization of moist convection for general circulation models, *Mon. Wea. Rev.*, **120**, 978-1002.
- Murphy, J., 1999: An evaluation of statistical and dynamical techniques for downscaling local climate, *J. Climate*, **12**, 2256-2284.
- Oki, T., and S. Kanae, 2006: Global hydrological cycles and world water resources, *Science*, **313**, no.5790, 1068-1072.
- Pan, H.-L. and W.-S. Wu, 1994: Implementing a mass flux convective parameterization package for the NMC medium-range forecast model, Preprints, 10th Conf. on Numerical Weather Prediction, Portland, OR, Amer. Meteor. Soc., 96-98.
- Parish, T.R. and J.J. Cassano, 2001: Forcing of the wintertime Antarctic boundary layer winds from the NCEP-NCAR global reanalysis, *J. Appl. Meteor.*, **40**, 810-821.
- Rockel, B., I. Meinke, J. Roads, W.J. Gutowski, Jr., R.W. Arritt, E.S. Takle, C. Jones, 2005: The inter-CSE Transferability study, *CEOP Newsletter*, **8**, 4-5.
- von Storch, H., H. Langenberg, and F. Feser, 2000: A spectral nudging technique for dynamical downscaling purposes, *Mon. Wea. Rev.*, **128**, 3664-3673.

Wilby, R.L., L.E. Hay, and G.H. Leavesley, 1999: A comparison of downscaled and raw GCM output: implications for climate change scenarios in the San Juan river basin, Colorado, *J. Hydrol.*, **225**, 67-91.

Figure Captions

Figure 1: Power spectra of kinetic energy at two different sigma levels. (a) $\sigma=0.864$: low troposphere and (b) $\sigma=0.147$: high troposphere. Black dashed lines indicate Reanalysis 2 (R2), blue solid lines are forecast simulation (FCST), and red dotted, green dotted, and black solid lines indicate CTL, TEMP1, and TEMP2, respectively. All spectra are averaged for 5 days from 6 March 1990.

Figure 2: Difference of 50hPa geopotential height between the control (CTL) and Reanalysis 2 (R2). The result is 3-day averaged from 6 Mar 1990.

Figure 3: Global RMSD of geopotential height at 17 pressure levels for CTL (dotted line), TEMP1 (solid line with open circles), and TEMP2 (solid line with closed squares), compared with R2. The result is 3-day averaged from 6 Mar 1990.

Figure 4: Global monthly mean air temperature at 2 meter surface over land in July 2001. (a) CRU observation, (b) Reanalysis 2, and (c) T248 simulation. Differences from CRU (a) of R2 and T248 are shown in (d) and (e), respectively.

Figure 5: Global distribution of monthly precipitation in January (left column) and July (right column) 2001. The top panels (a, b) are CRU, the next panels (c, d) show GPCP, then R2 (e, f), T248 nudged simulation results are shown (g, h), and finally T248 forecast simulation results (i, j).

Figure 6: Seasonality of global averaged precipitation, over whole (a) globe and (b) land. GPCP is used in (a), and CRU is used in (b). Black solid lines are assigned for both observations. Blue lines and green lines indicate R2 and T248, respectively.

Figure 7: Global distribution of correlation coefficient of (a, b) Reanalysis 2 and (c, d) T248 with daily GPCP precipitation in (a, c) January and (b, d) July 2001.

Figure 8: Correlation coefficient of R2 and T248 daily precipitation with GPCP are globally averaged in each month. A solid line and a dotted line indicate Reanalysis 2 and T248, respectively.

Figure 9: Monthly mean surface wind speed at 10 m over North America. (a) Reanalysis 2, (b) T248, and (c) NARR are shown for July 2001.

Figure 10: Daily mean surface temperature anomaly from monthly average over North America. (a) Reanalysis 2, (b) T248, and (c) NARR are shown for 29 July 2001.

Figure 11: Spatial distribution of correlation coefficient of Reanalysis 2 (first and third left columns) and T248 (second and fourth left columns) with AMeDAS surface observations, in January (left eight panels) and July (right eight panels) 2001. From the top, (a-d) surface wind speed, (e-h) surface temperature, (i-l) humidity, and (m-p) precipitation are shown.

Figure 12: Temporal variations of Reanalysis 2 (thin solid line with open square), T248 (black thick line with closed circle), and AMeDAS observation (gray thick line) are compared for (a) surface wind speed, (b) surface temperature, (c) surface humidity, and (d) precipitation.

Figure 13: Daily averaged temperature anomalies (shades), winds (arrows), and topography (gray contour; 300 m interval and 0 m line are omitted). Left and right columns show Reanalysis 2 and T248-nudged runs, respectively. (a, b) Santa Ana wind in Southern California on 3 January 2001, (c, d) Mistral wind in West Europe on 22 December, 2001, and (e, f) katabatic winds in Antarctic Peninsula on 29 July 2001 are shown.

Figure A: Results of the sensitivity experiments. Gray lines denote three

experiments in the main text, CTL, TEMP1, and TEMP2 (same as the lines in Figure 3). Black lines indicate additional experiments of L1000 (open squares), L1000F (open circles), ALP05 (crosses), and ALP02 (closed circles).

Table 1. Specification of experiments

	Damping	Weighting Coefficient (α)	Nudging Scale (L)	Comparable with
CTL	UV	0.9	2000 km	
TEMP1	UV and T	0.9	2000 km	
TEMP2	UV and T	Attenuating Function	2000 km	
L1000	UV	0.9	1000 km	CTL
L1000F	UV and T	Attenuating Function	1000 km	TEMP2
ALP05	UV and T	0.5	2000 km	TEMP1
ALP2	UV and T	2.0	2000 km	TEMP1

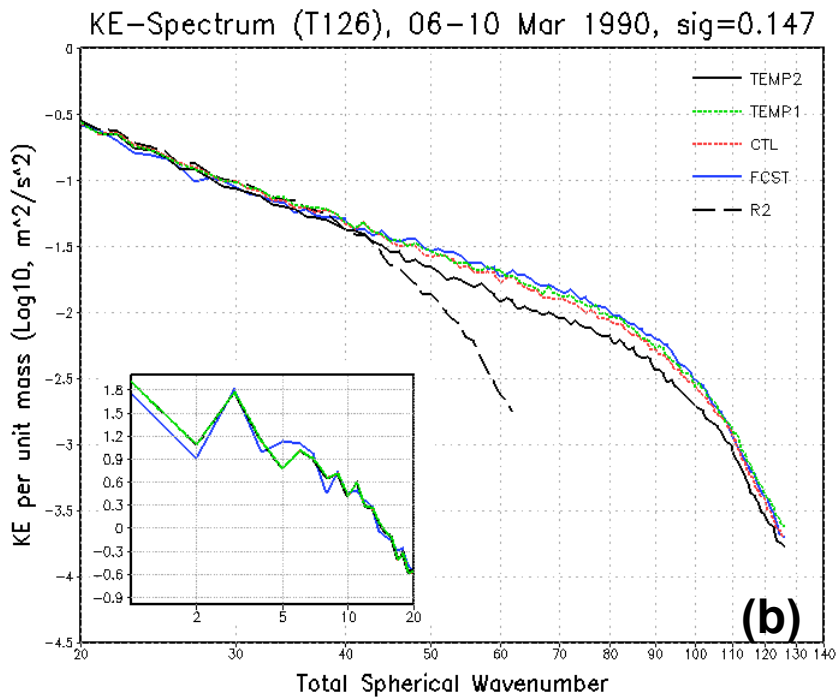
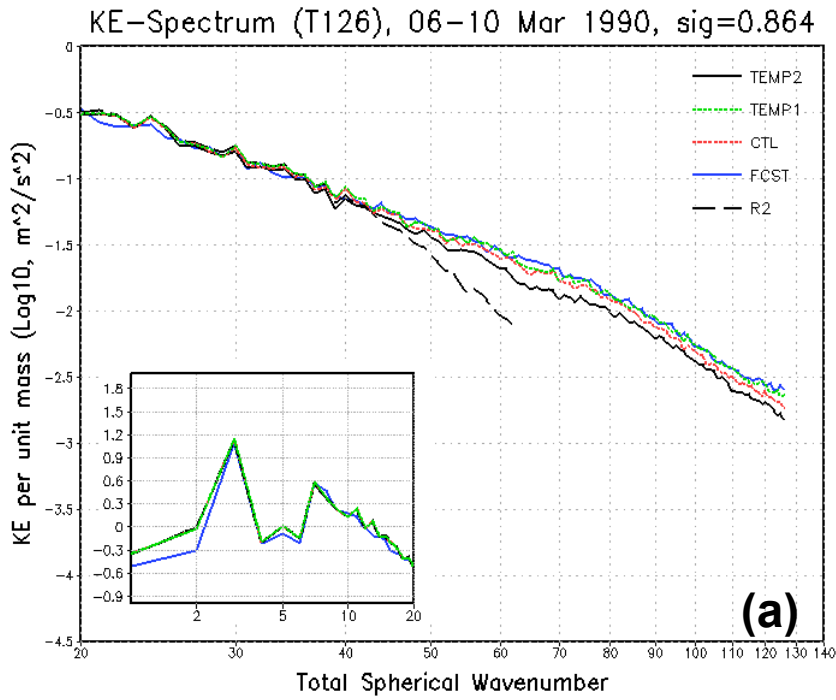


Figure 1: Power spectra of kinetic energy at two different sigma levels. (a) sigma=0.864: low troposphere and (b) sigma=0.147: high troposphere. Black dashed lines indicate Reanalysis 2 (R2), blue solid lines are forecast simulation (FCST), and red dotted, green dotted, and black solid lines indicate CTL, TEMP1, and TEMP2, respectively. All spectra are averaged for 5 days from 6 March 1990.

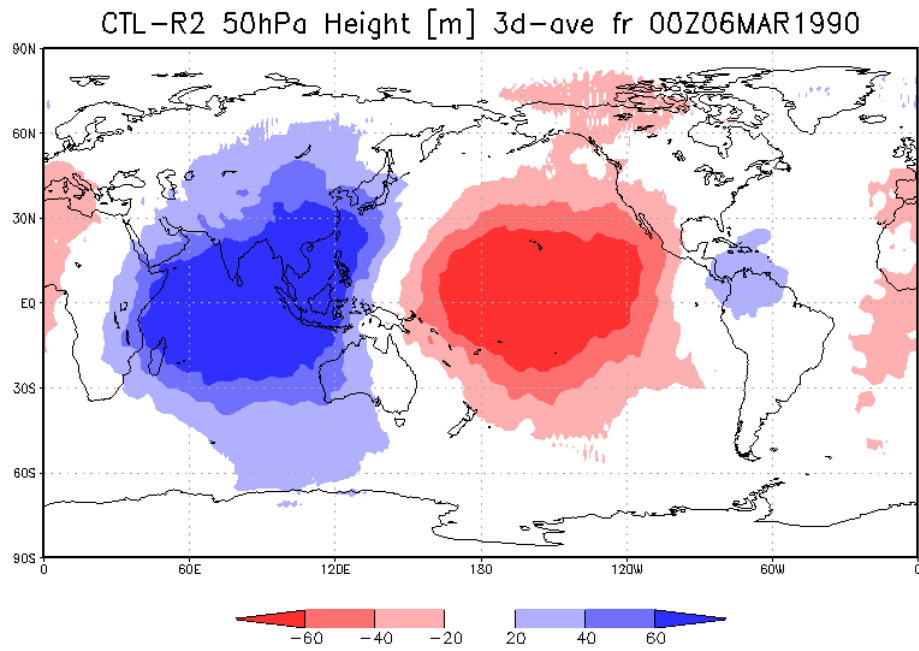


Figure 2: Difference of 50hPa geopotential height between the control (CTL) and Reanalysis 2 (R2). The result is 3-day averaged from 6 Mar 1990.

Glb RMSD Height, 3d-ave fr 06MAR1990

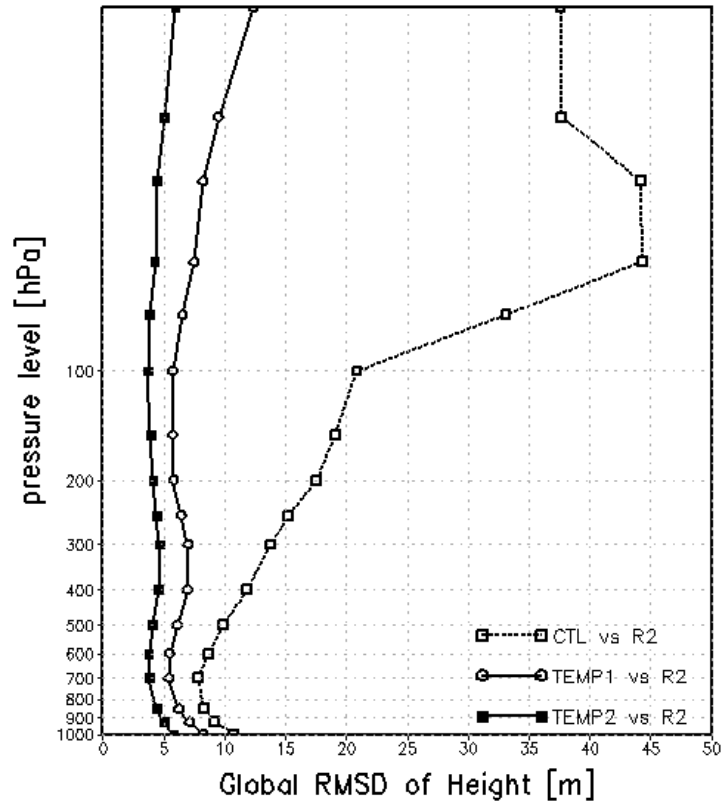


Figure 3: Global RMSD of geopotential height at 17 pressure levels for CTL (dotted line), TEMP1 (solid line with open circles), and TEMP2 (solid line with closed squares), compared with R2. The result is 3-day averaged from 6 Mar 1990.

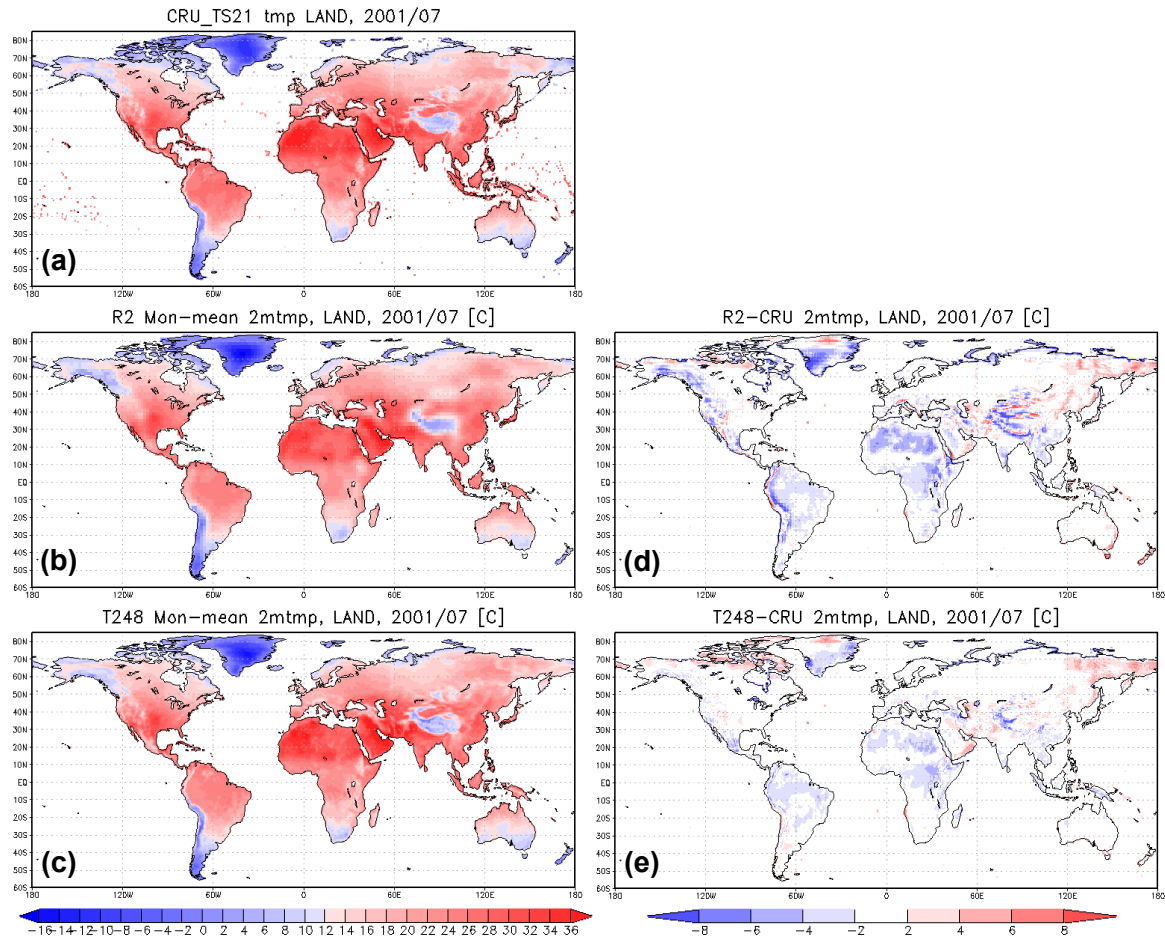


Figure 4: Global monthly mean air temperature at 2 meter surface over land in July 2001. (a) CRU observation, (b) Reanalysis 2, and (c) T248 simulation. Differences from CRU (a) of R2 and T248 are shown in (d) and (e), respectively.

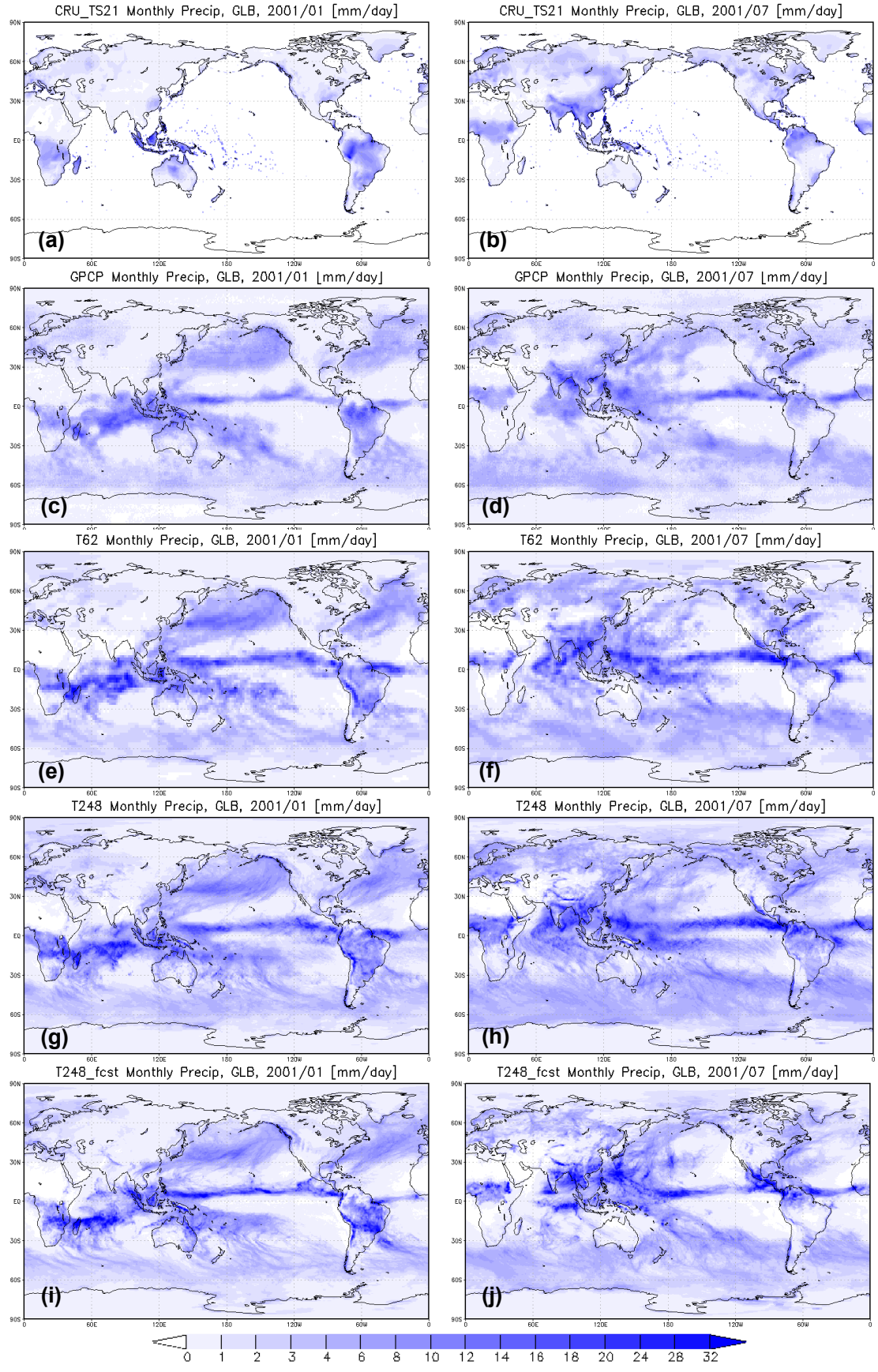


Figure 5: Global distribution of monthly precipitation in January (left column) and July (right column) 2001. The top panels (a, b) are CRU, the next panels (c, d) show GPCP, then R2 (e, f), T248 nudged simulation results are shown (g, h), and finally T248 forecast simulation results (i, j).

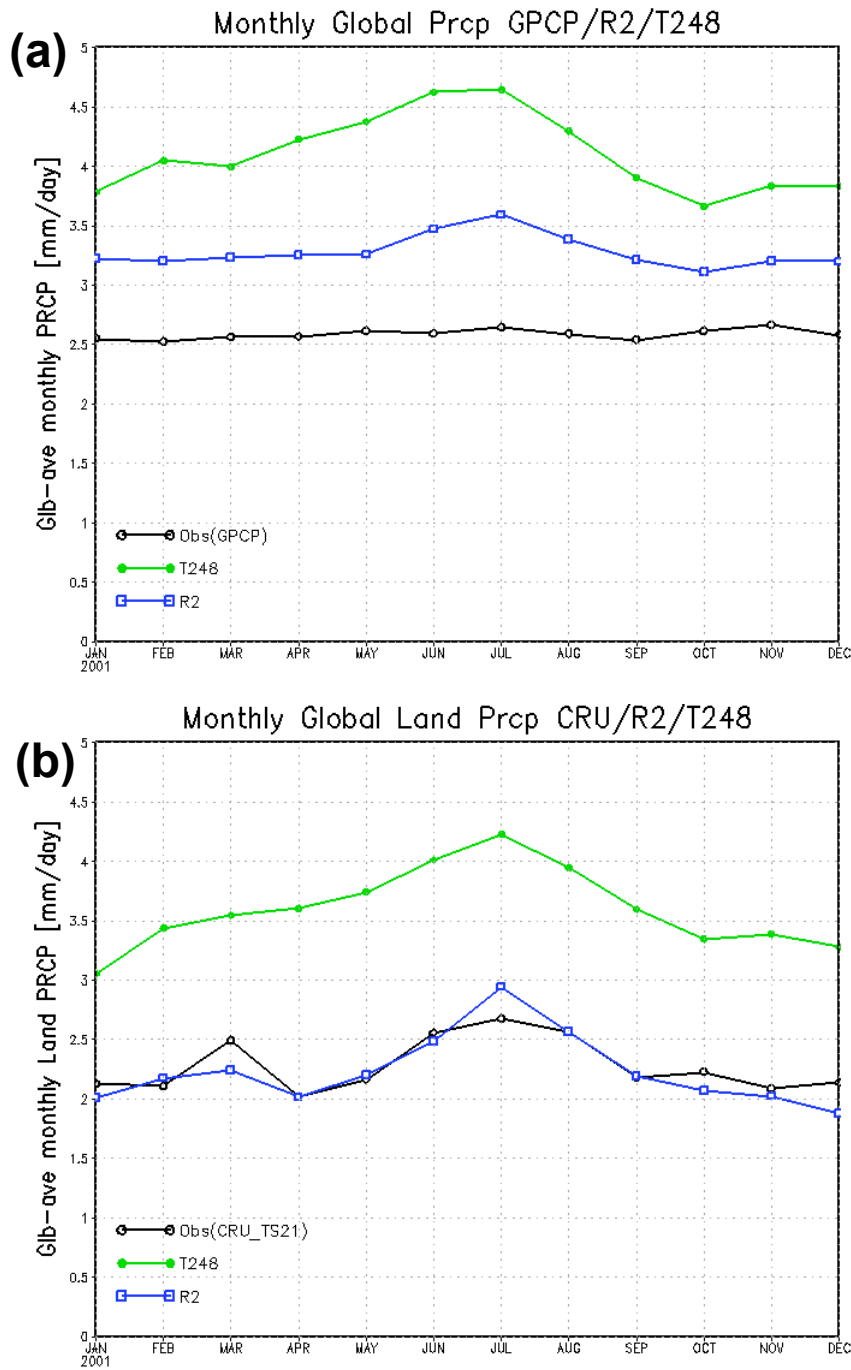


Figure 6: Seasonality of global averaged precipitation, over whole (a) globe and (b) land. GPCP is used in (a), and CRU is used in (b). Black solid lines are assigned for both observations. Blue lines and green lines indicate R2 and T248, respectively.

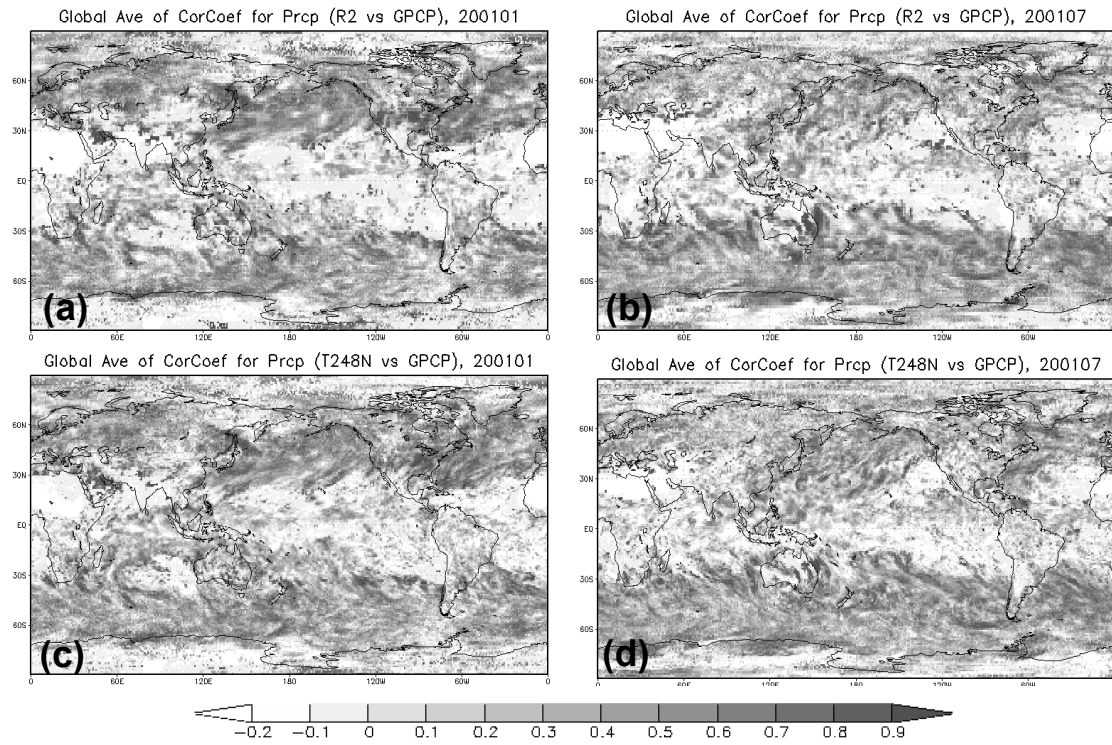


Figure 7: Global distribution of correlation coefficient of (a, b) Reanalysis 2 and (c, d) T248 with daily GPCP precipitation in (a, c) January and (b, d) July 2001.

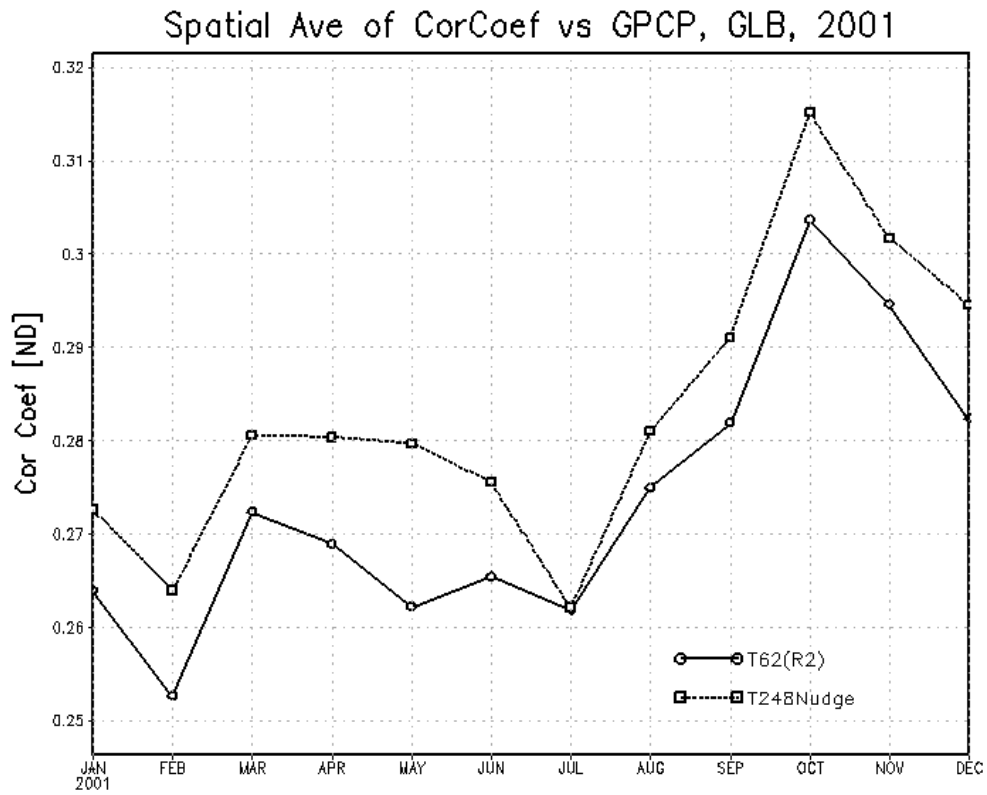


Figure 8: Correlation coefficient of R2 and T248 daily precipitation with GPCP are globally averaged in each month. A solid line and a dotted line indicate Reanalysis 2 and T248, respectively.

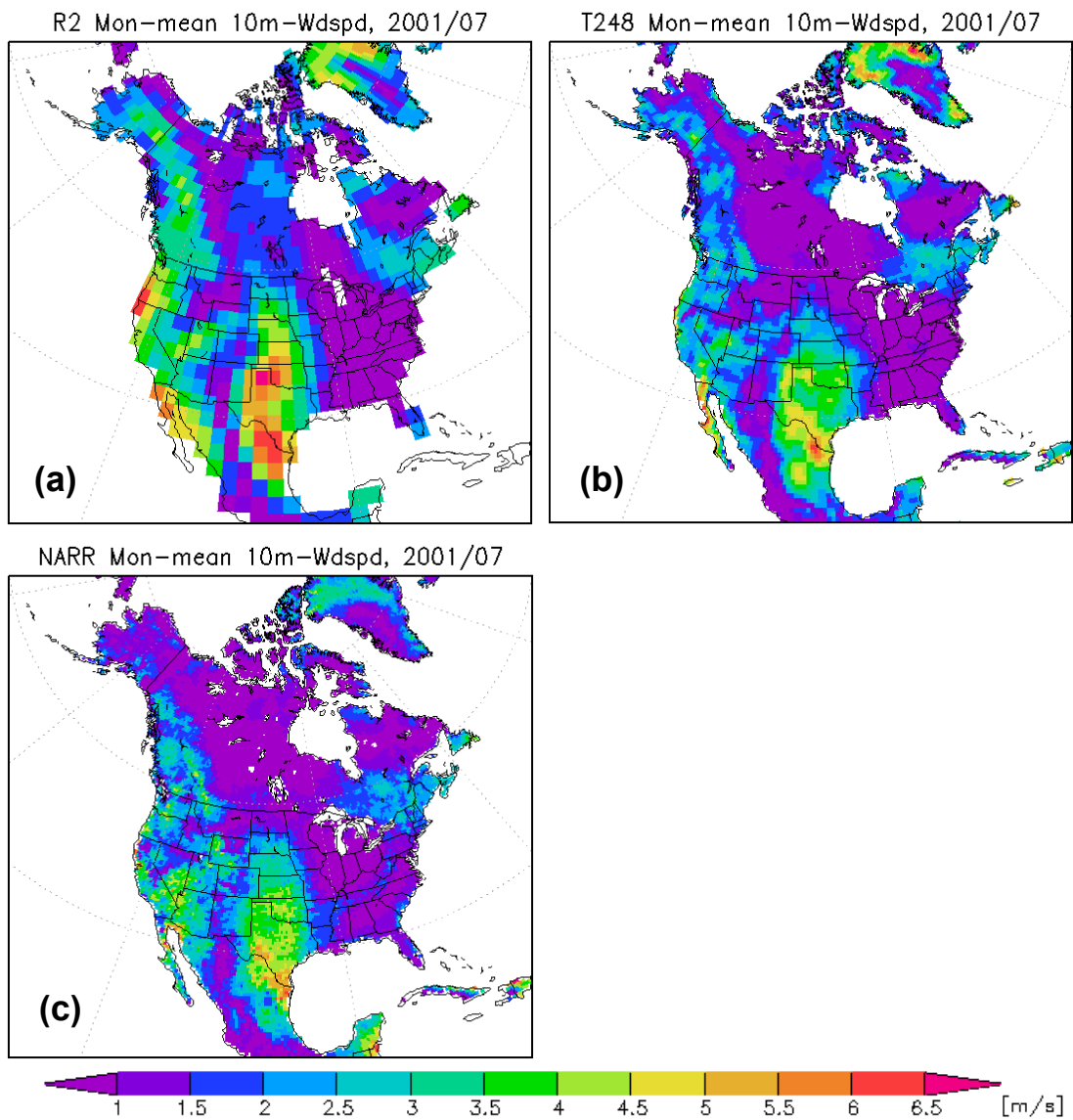
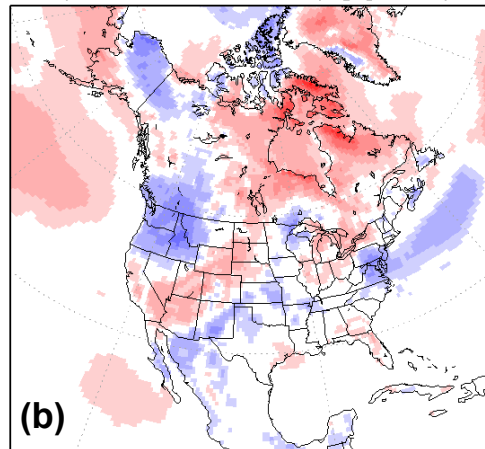
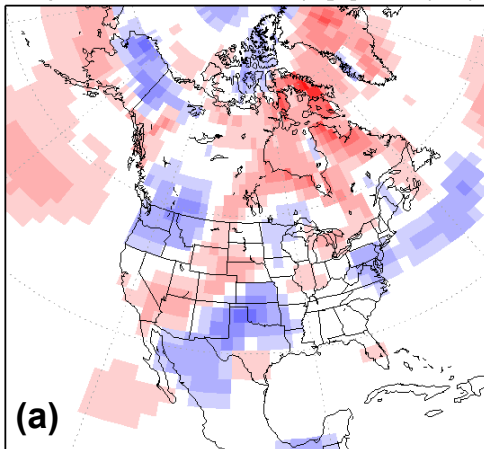


Figure 9: Monthly mean surface wind speed at 10 m over North America. (a) Reanalysis 2, (b) T248, and (c) NARR are shown for July 2001.

R2 Daymean-Monmean 2mtmp [K], 2001/07/29 T248 Daymean-Monmean 2mtmp [K], 2001/07/29



NARR Daymean-Monmean 2mtmp [K], 2001/07/29

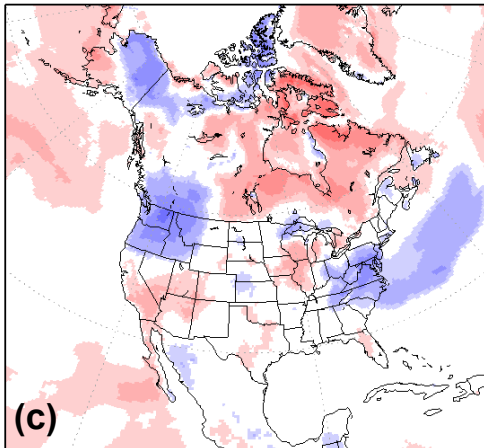


Figure 10: Daily mean surface temperature anomaly from monthly average over North America. (a) Reanalysis 2, (b) T248, and (c) NARR are shown for 29 July 2001.

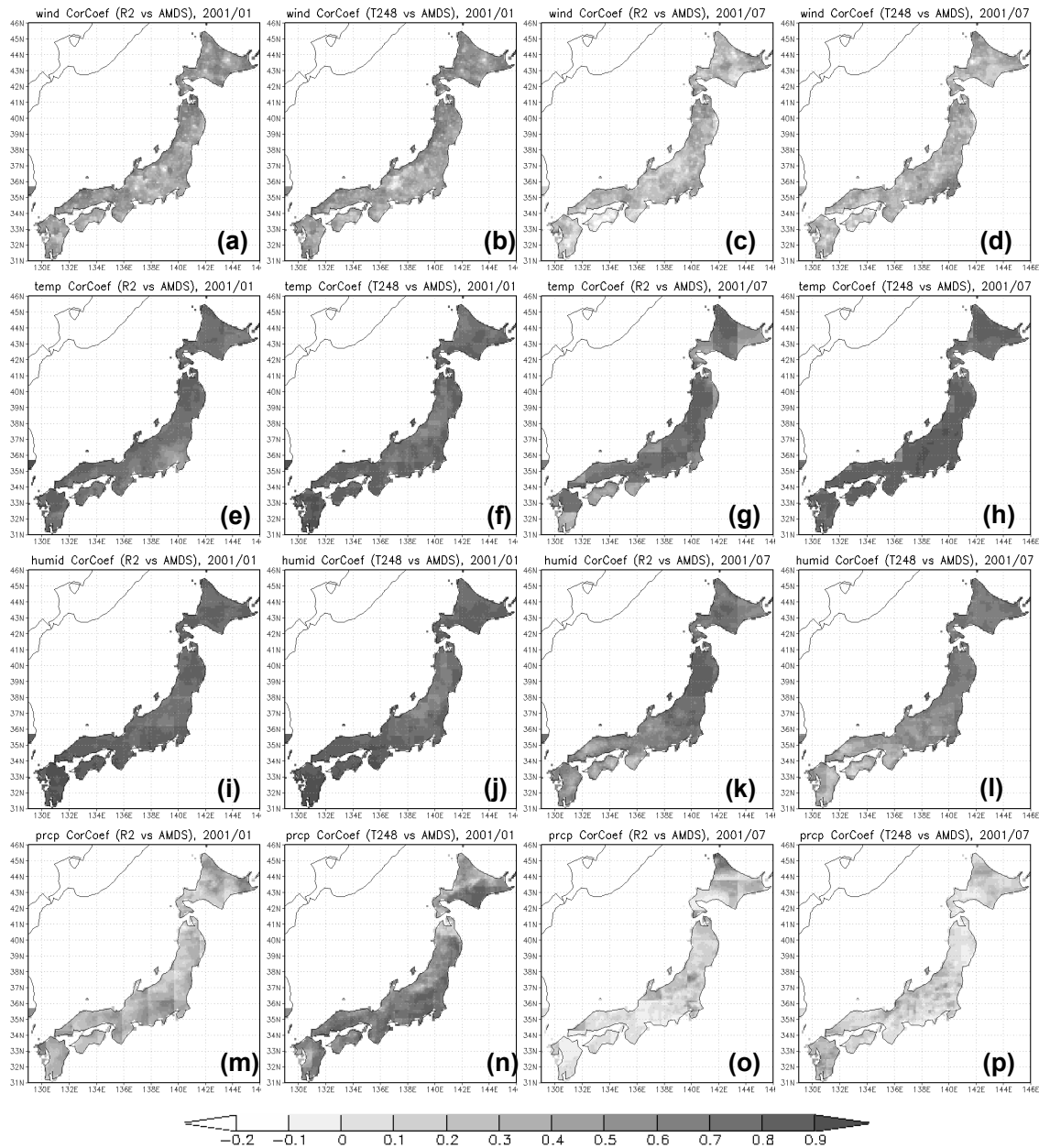


Figure 11: Spatial distribution of correlation coefficient of Reanalysis 2 (first and third left columns) and T248 (second and fourth left columns) with AMeDAS surface observations, in January (left eight panels) and July (right eight panels) 2001. From the top, (a-d) surface wind speed, (e-h) surface temperature, (i-l) humidity, and (m-p) precipitation are shown.

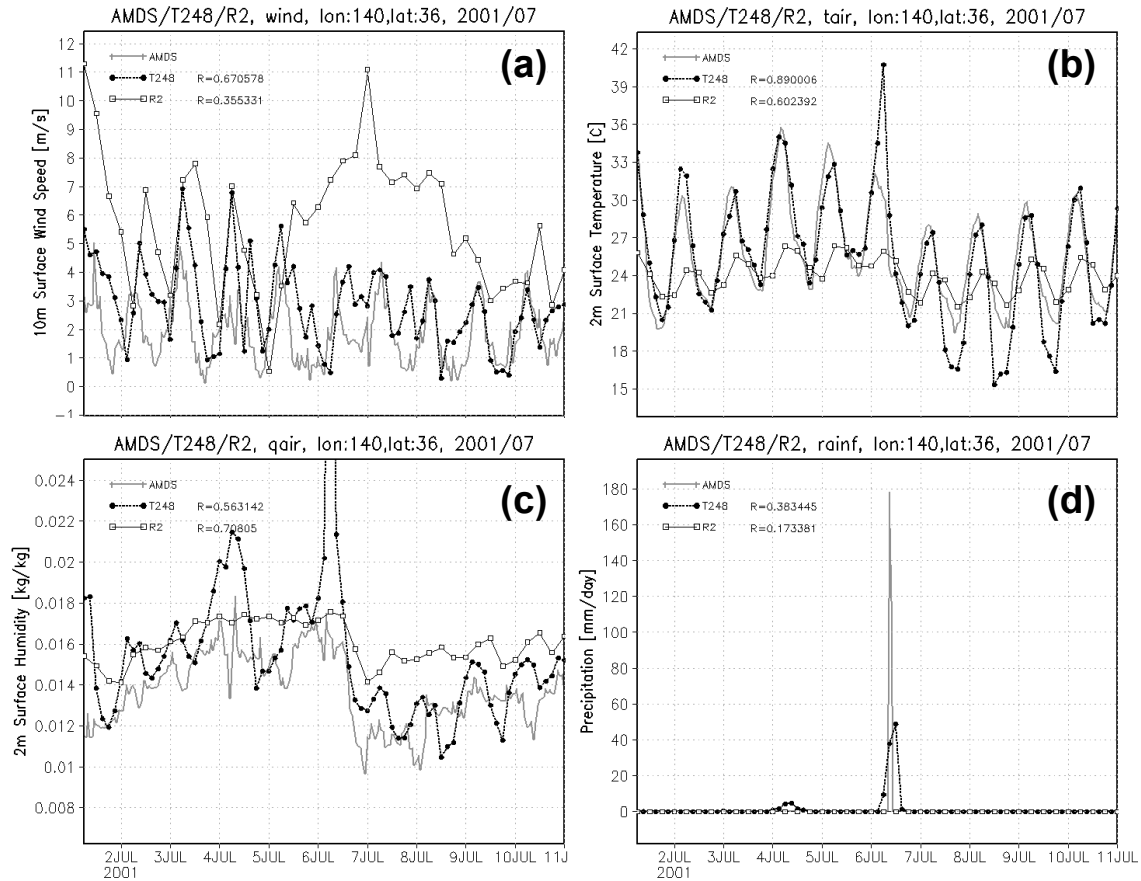


Figure 12: Temporal variations of Reanalysis 2 (thin solid line with open square), T248 (black thick line with closed circle), and AMeDAS observation (gray thick line) are compared for (a) surface wind speed, (b) surface temperature, (c) surface humidity, and (d) precipitation.

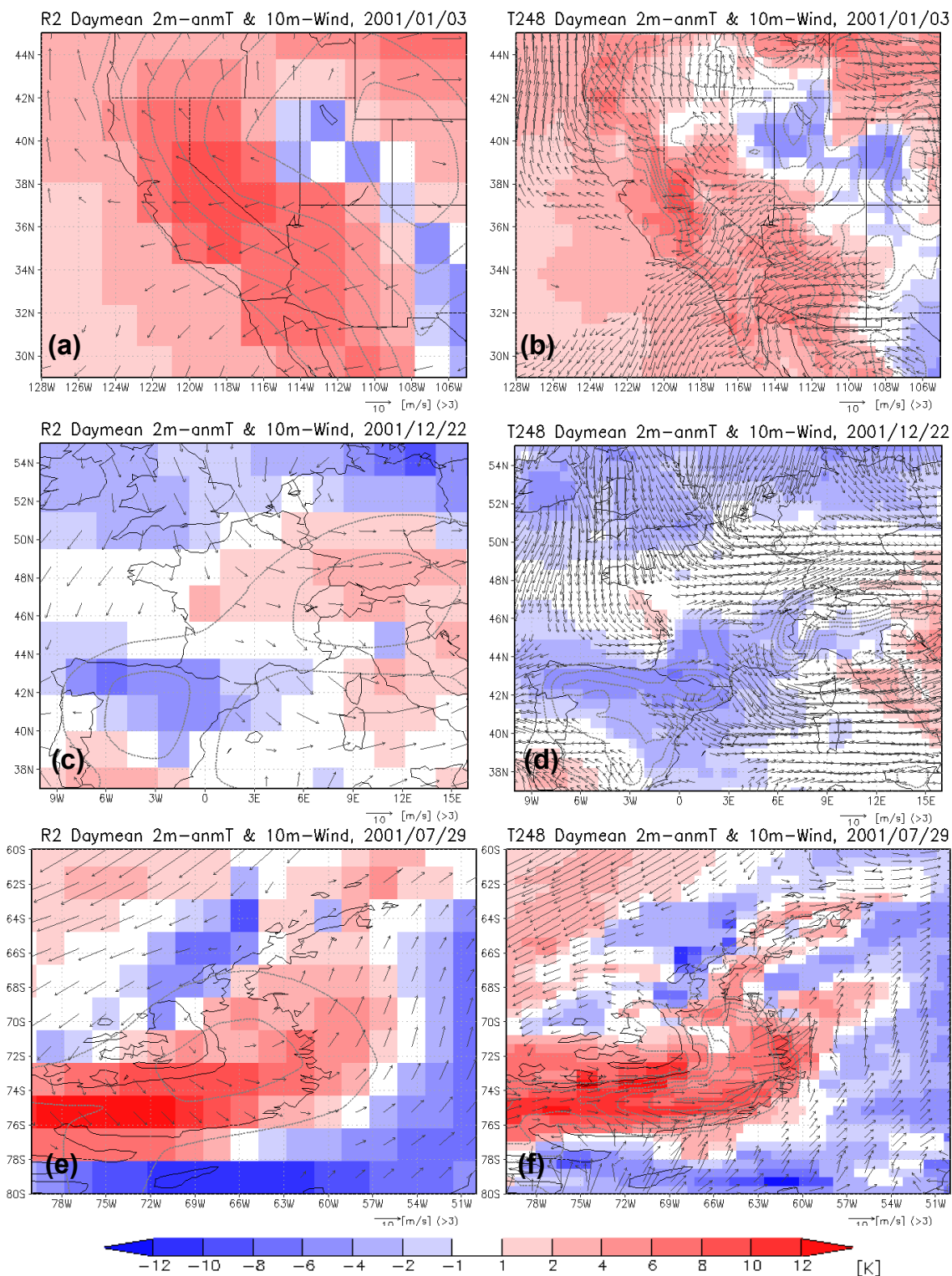


Figure 13: Daily averaged temperature anomalies (shades), winds (arrows), and topography (gray contour; 300 m interval and 0 m line are omitted). Left and right columns show Reanalysis 2 and T248-nudged run, respectively. (a, b) Santa Ana

wind in Southern California on 3 January 2001, (c, d) Mistral wind in West Europe on 22 December, 2001, and (e, f) katabatic winds in Antarctic Peninsula on 29 July 2001 are shown. Number of arrows is horizontally cropped to 1/4 in (f).

Glb RMSD Height, 3d-ave fr 06MAR1990

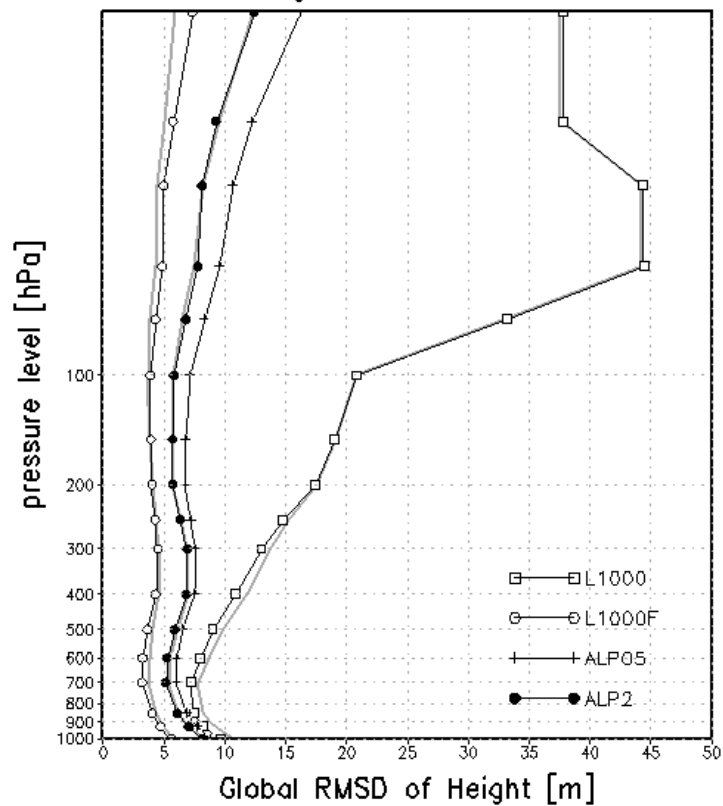


Figure A: Results of the sensitivity experiments. Gray lines denote three experiments in the main text, CTL, TEMP1, and TEMP2 (same as the lines in Figure 3). Black lines indicate additional experiments of L1000 (open squares), L1000F (open circles), ALP05 (crosses), and ALP02 (closed circles).